



# Two-Dimensional Electronic Spectroscopy Reveals Excitation Energy-Dependent State Mixing during Singlet Fission in a Terrylenediimide Dimer

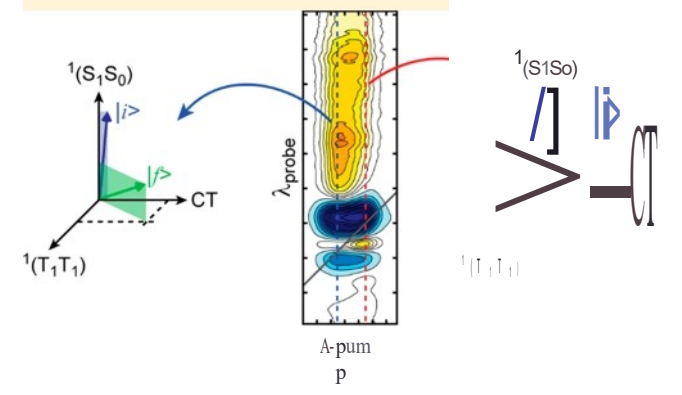
Aritra Mandal & Michelle Chen / Eileen D. Foszczt Jonathan D. Schultz Nicholas M. Keams Ryan M. Young, \*t'e Martin T. Zanni / Cr> and Michael R Wasielewski \*t'o

t Dep artment of Chemistry and Institute for Sustainability and Energy at NorthwesternNorthwestern University, Evanston Illinois 60208-3113, United States

\*Department of Chemistry, University of Wisconsin-Madison Madison Wisconsin 53706, United States

**0** Supporting Information

ABSTRACT: Singlet fission (SF) is a spin-allowed process in which a singlet exciton, <sup>1</sup>(S<sub>1</sub>S<sub>0</sub>), within an assembly of two or more chromophores spontaneously down-converts into two triplet excitons via a multiexciton correlated triplet pair state, <sup>1</sup>(T<sub>1</sub>T i). To elucidate the involvement of charge transfer (CT) states and vibronic coupling in SF, we performed 2D electronic spectroscopy (2DES) on dilute solutions of a covalently linked, slip-stacked terrylene-3,4: 11,12-bis-(dicarboximide) (TDI) dimer. This dimer undergoes efficient SF in nonpolar 1,4-dioxane and symmetry-breaking charge separation in polar dichloromethane. The various 2DES spectral features in 1,4-dioxane show different pump wavelength dependencies, supporting the presence of mixed states



with variable <sup>1</sup>(S<sub>1</sub>S<sub>0</sub>), <sup>1</sup>(T<sub>1</sub>T<sub>1</sub>) and CT contributions that evolve with time. Analysis of the 2DES spectra in dichloromethane reveals the presence of a state having largely <sup>1</sup>(T<sub>1</sub>T<sub>1</sub>) character during charge separation. Therefore, the <sup>1</sup>(T<sub>1</sub>T<sub>1</sub>) multiexciton state plays an important role in the photophysics of this TDI dimer irrespective of solvent polarity.

# INTRODUCTION

Singlet fission (SF) is a spin-allowed process in which a singlet exciton in an assembly of two or more chromophores spontaneously down-converts into two triplet excitons. Because of its potential to increase the efficiency of single junction solar cells from the Shockley-Qieisser limit of 33% to 45%, studies of SF have seen an upsurge in the past decaded. For SF to occur, the energy of the singlet excitonic state (S1) must be approximately twice that of the lowest triplet excitonic state (T1). Additionally, the SF efficiency depends critically on the coupling between the neighboring chromophores, dictated largely by their relative distance and spat  $^{10}$  n.  $^{5}$   $^{9}$ 

In the first step of SF, a singlet exciton involving two adjacent molecules,  ${}^1(S_1S_0)$ , produces a multiexciton correlated triplet pair state, I [ | 1 | 1), having an overall singlet spin with a rate constant around  $10^9$ -  $10^{13}$ -s  $^1.3$  The  ${}^1(T_1T_1)$  state subsequently undergoes spin dephasing to generate two independent triplet excitons, T + 11, usually in a few nanoseconds3. Two alternative mechanisms have been proposed for the primary SF event. One mechanism involves direct conversion of  ${}^1(S_1S_0)$  to  ${}^1(T_1T_1)$  via a two-electron transfer,  ${}^1$  while the other involves two sequential single-electron transfer events.  ${}^1$  In the latter case, the charge

transfer (CT) state between the two adjacen,t electronically coupled chromophores plays a pivotal role; however, whether the CT state acts as an intermediate or couples the singlet and correlated triplet pair states via superexchange mechanism remains unclear in many cases. Moreove,r recent studies have suggested that vibronic cougling can mix  $^{1}(S_{1}S_{0})$  and  $^{1}(T_{1}T_{1})$  resulting in efficient SF.- Despite a wide range of experimental and theoretical investigations, several key mechanistic details of the primary SF event, particularly the exact roles of CT state and vibronic coupling, are poorly understood.

Efficient SF has been observed in thin films, single crystals and covalent dimers of organic chromophores like polyacenes  $^{1}\stackrel{\text{RP}}{=} 2$  30 rylenes  $^{5,6,89,31}$  diketopyrrolopyrroles  $^{3}$  1,3-diphenyl-isobenzourans,34-36 etc. Owing to their precise control over interchromophore orientation, covalent dimers are often used to study the SF mechanism. Our previous work showed efficient SF in a covalently linked n-stacked dimer of terrylene-3,4:11,12-bis(dicarboximide) (TDI) where the two parallel TDI molecules are slipped relative to one another along their N-N axes by about 8 A.  $^{6,37}$  The CT state energy of

Received: August 11, 2018 Published: December 2, 2018

MMM

this slip-stacked TDI dimer is also very close to the energies of the  ${}^{1}(S S_{d})$  and  ${}^{1}(T T)_{1}$  st ates. Consequently, its photophysics depend strongly on solvent polarity with 1 (T 1 T 1) formation favored in nonpolar solvents, while symmetry-breaking charge separation (SB-CS) is favored in polar solvents and produces the TDP -TD • CT state. Our recent study of a slip-stacked TDI dimer (XanTDI<sub>2</sub>) using femtosecond transient IR absorption spectroscopy clearly showed that the multiexciton state has vibrational modes characteristic of the T1 state alongside those specific to TDi-•.37 The simultaneous presence of CT and triplet state features in both polar dichloromethane (DCM) and nonpolar 1,4-dioxane throughout the multiexciton state lifetime suggests that this state is of mixed character including contributions from the CT and  $^{1}(T_{1}T_{1})$  states.

In the present worlc, we investigate the multiexciton state in XanTDI<sub>2</sub> using two-dimensional electronic spectroscopy (2DES) to further understand the relationships among the  $^{1}(S_{1}S_{0})$ . CT and  $^{1}(T_{1}T_{1})$  st ates. We focus on unraveling the roles of CT states and vibronic coupling in the primary event of SF using 2DES on XanTD I<sub>2</sub> and its monomeric reference compound XanTDI. 2DES measurements on dilute XanTD!z solutions in nonpolar1,4-dioxane and polar DCM demonstrate that, in general, the excited electronic states of this molecule have mixed (S,S), (T,T) and CT contributions. Moreover, in 1,4-dioxane, the nature of the mixture in the initially excited and the intermediate states are critically dependent on the excitation wavelength due to strong influence of vibronic coupling. On the other hand, an intermediate state with significant <sup>1</sup> (T <sub>1</sub>T <sub>1</sub>) character is observed during SB-CS in DCM regardless of excitation wavelength.

# RESULTS AND DISCUSSION

Stead y-Sta te Spe ct rosco py. The linear UV-vis absorption spectrum of XanTDI in DCM (Figure 1) shows that the 0-0 and 0-1 vibronic bands are centered at 656 and 602 nm, respectively. The 0-0 and 0-1 vibronic bands for XanTDI2 in 1,4-dioxane and DCM are red-shifted by 0-3 nm compared to **XanTDI.** The intensity ratio of the vibronic peaks (0-1/0-0)increases and the spectra broaden in the dimer compared to the monomer. Electronic coupling between the chromophores in this slip-stacked dimer is relatively weak due to imperfect overlap of their n-systems; however, the energetic proximity

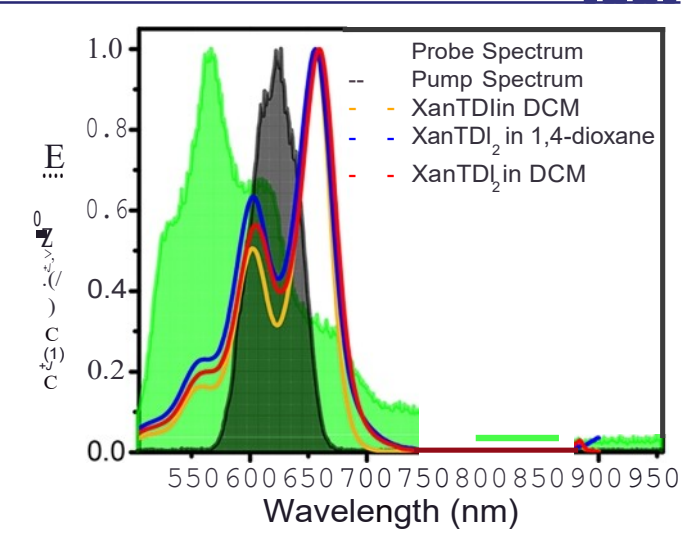


Figure 1. Comparison of linear UV-vis absorption spectra of XanTDI2 in 1,4-dioxane (blue) and DCM (red) with that of XanTDI in DCM (orange). All these spectra are normalized to the peak of the 0-0 vibronic band centered at -656 nm. Normalized spectra for the pump and probe pulses used in 2DES are shown by transparent black and green traces, respectively.

and possibility of coupling between the  ${}^{1}(S_{1}S_{0})$ ,  ${}^{1}(T_{1}T_{1})$  and CT states together with vibronic coupling complicates interpretation of the linear absorption spectra of XanTDI<sub>2</sub>.

Two-Dimensional Electronic Spectroscopy. Experimental implementation of 2DES requires three time-ordered femtosecond visible pulses. The 2DES experiments were performed in the pump-probe geometry with a pulse shaper to generate two time-ordered pump pulses in which the interpulse spacing is -r<sub>1</sub> and the waiting time between the second pump pulse and the probe pulse is -r<sub>2</sub> (see Methods).<sup>3</sup> The pump and the probe pulses were polarized parallel to each other for all the 2DES spectra shown in this work unless otherwise mentioned. Figure 2 shows 2DES spectra XanTDI2 in 1,4-dioxane as a function of -r2 (spectra at additional -r<sub>2</sub> values are given in Figure S3). The ground-state bleach (GSB) and stimulated emission (SE) signals in 2DES have a negative sign and are plotted using blue contour lines; whereas, the excited-state absorption (ESA) signals with positive signs are plotted using red contours. At  $-r_2 = 3$  ps. we observe the GSB signals on the diagonal at 656 and 602 nm, corresponding to the 0-0 and 0-1 vibronic bands, respectively. Cross peaks between these two transitions are also observed The ESA signal due to the S<sub>0</sub> S<sub>1</sub> transition is detected in the 2DES spectrum centered at ,\robe = 890 nm. The 2DES spectra presented here (Figure 2) are convolutions of the third-order nonlinear response of XanTDI2 with the pump and the probe pulses. Given that the pump pulse spectrum partially covers both the 0-0 and 0-1 vibronic transitions and cuts off close to the peak of the stronger 0-0 vibronic transition, the overall GSB and singlet ESA signals appear as one peak, elongated along the pump wavelength axis. In order to avoid artifacts at the edge of the pump pulse spectrum, it was not deconvoluted from the 2DES spectra. Visible one-dimensional femtosecond transient absorption (fsTA) spectroscopy demonstrates generation of  ${}^{1}(T_{1}T_{1})$ from  ${}^{1}(S_1S_0)$  in 1,4-dioxane in -r = 2.7 ps.  ${}^{37}$  Consequently, the ESA feature arising due to the  $T_0$   $T_1$  transition from the  ${}^{1}(T_{1}T_{1})$  state is observed in the **XanTDI<sub>2</sub>** 2DES spectrum in

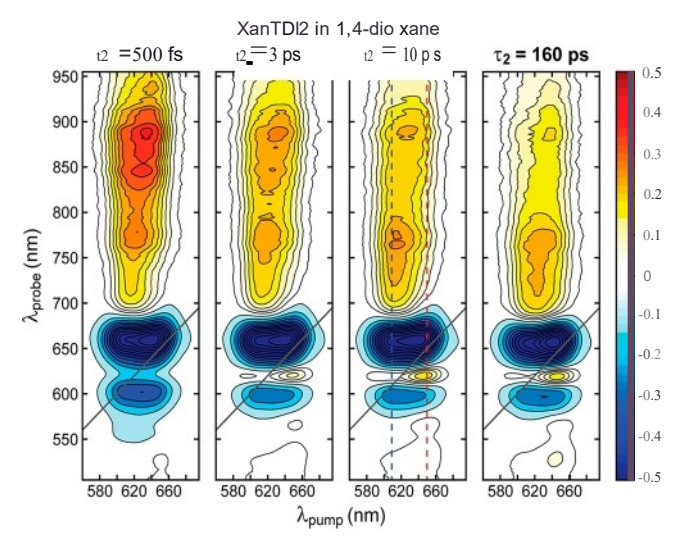


Figure 2. 2DES spectra of XanTD  $I_2$  in 1,4-dioxaneat waiting times of 500 fs, 3 ps, 10 ps and 160 ps. The spectrum at each waiting time is normalized to the corresponding peak of the ground-state bleach signal. To contrast the weaker signals, a color gradient is used for contour levels between - 0.5 and +0.5 only. The blue and red dashed lines on the 2DES spectra at  $-r_2 = 10$  ps indicate the pump wavelength slices used for kinetic analysis.

621 dioxane at i-2=3 ps centered at (JpumP'A probe) = (651 nm). Even though (T I) and the independent T states, have comparable spectra, the monoexponential  ${}^{1}(T_{1}T_{1})$  population decay to ground state in -r = 1.34 ns of **XanTDl**<sub>2</sub> in 1,4-dioxane is evidence against separation of the multi-exciton state into two independent triplet excitons. As a result, we observe these transient signals in the IDES spectrum at the longest waiting time accessible in our measurements (160 ps).

Figure 3 shows 2DES spectra of XanTDI<sub>2</sub> in DCM as a function of  $\cdot_2$  (spectra at additional  $\cdot_2$  are given in Figure S4). At  $\cdot_2$  = 6 ps, GSB bleach features corresponding to the 0-0 and

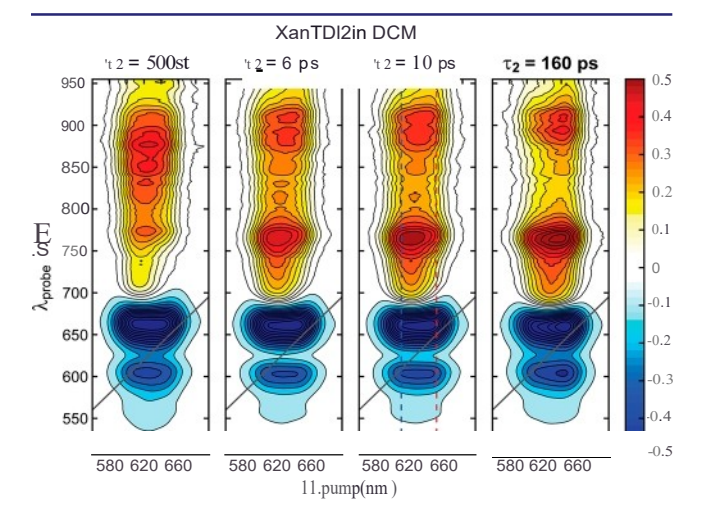


Figure 3. 2DES spectra of  $XanTDI_2$  in DCM at waiting ti.mes of 500 fs, 3 ps, 10 ps and 160 ps. The spectrum at each waiting ti.me is normalized to the corresponding peak of the ground-state bleach signal. To contrast the weaker signals, a color gradient is used for contour levels between - 0.5 and +0.5 only. The blue and red dashed lines on the 2DES spectra at - $r_2$ = 10 ps indicate the pump wavelength slices used for kinetic analysis.

0-1 vibronic bands and ESA feature arising due to the  $S_0$   $S_1$  transition are observed similar to  $\mathbf{XanTDl}_2$  in 1,4-dioxane. FsTA spectroscopy reports the occurrence of SB-CS for XanTDI<sub>2</sub> in DCM in -res = S.S ps. 37 Co nseq uently,an ESAdue to  $\mathbf{m}$  1+• is observed at (,\,ump, A.probe) = (622 nm, 765 nm) in the 2DES spectrum of  $\mathbf{XanTDI}_2$  in DCM at  $\mathbf{h}_2 = 6$  ps. Because charge recombination of  $\mathbf{TDl}^2$  -TDI-• occurs in -rcR = 437 ps for  $\mathbf{XanTDI}_2$  in DCM,3<sup>7</sup> these spectral signatures are present in the 2DES spectrum at  $\mathbf{h}_2 = 160$  ps. Additionally, a solution of  $\mathbf{XanTDI}_2$  in DCM at a concentration similar to  $\mathbf{XanTDI}_2$  does not show any spectral signatures arising from the

state or **m** r+• in the 2DES spectra (Figure SS), confirming the intramolecular origin of the spectral features in **XanTDlz**.

Interestingly, ESA due to  $m \ r^{+\bullet}$  is also observed at (JpumP' A.probe)= (613 nm, 764 nm) in the 2DES spectra of XanTDl  $_2$  in 1,4-dioxane at all the measured waiting times beyond 100 fs (-.2 = 100 fs to 160 ps), albeit weaker than in DCM. Notably, the ESA features due to the  $^1(T_1T_1)$  and  $^1(T_1T_2)$  and  $^1(T_1T_2)$  states are centered at different pump wavelengths at all waiting times between LS and 160 ps in 1,4-dioxane. Also, all the peaks in the 2DES spectra red-shift slightly along the pump wavelength axis as a function of -.2 due to relaxation of the excited-state population back to the ground state.

Previouswork on similar TDI dimers suggested the presence of an equilibrium between the  ${}^{1}(S_{1}S_{0})$  state and the  ${}^{1}(T_{1}T_{1})$ state during SF in nonpolar solvents.<sup>6</sup> Further studies of XanTDI<sub>2</sub> in 1,4-dioxane recognized two possible scenarios during SF: an equilibrium between the (S<sub>1</sub>S<sub>0</sub>), (T<sub>1</sub>T<sub>1</sub> and CT states that allows population transfer but does not alter the electronic states themselves, or significant mixing of the (SS), (TT) and CT electronic states so that the initial excitation created is a superpositin of eigenstates. Femtosecond transient mid-IR absorption data ultimately favored the latter scenario<sup>37</sup> Because the ESA due to TDI<sup>o</sup> appears in the 2DES spectra within the instrument response time, and is centered at a different pump wavelength at all waiting, times compared to the (TT) ESA, while ESA from the (SSo) state is observed at b 1 1 pump wavelengths, existen 1 of of these equilibria between pure (SS), (TT) and CT electronic states can be ruled out. Equilibria between the pure electronic states would have created an initial population in the  ${}^{1}(S_{1}S_{0})$ state after first two interactions with the pump pulses in a 2DES measurement. Consequently, it would have caused the ESA features due to all the pure electronic states to be centered at the same pump wavelength as depicted in Figure 4 (right). Thus, the 2DES spectral features for XanTDl<sub>2</sub> in 1,4-dioxane, particularly the pump wavelength dependence of the ESA arising from the  ${}^{1}(T_{1}T_{1})$  and CT states, can only be explained by significant  ${}^{1}(S_{1}S_{0})$ ,  ${}^{1}(T_{1}T_{1})$  and CT state mixing. However, electronic coupling between the pure electronic states of this system is weak, as reflected by the minor differences in the linear absorption spectra of XanTDI<sub>2</sub> and XanTDI. Strong electronic coupling noticeably alters the linear absorption peak positions and intensities in covalent TDI dimers with greater n-system overlap. Owing to the close proximity of the <sup>1</sup>(S<sub>1</sub>S<sub>0</sub>), 1 (T1T1) and CT state energies,6 st rongvibronic coupling is the most likely cause of significant state mixing of  ${}^{1}(S_1S_0)$ ,  ${}^{1}(T_1T_1)$ and CT. Moreover, the relative contributions of these states to the resulting mixed electronic states accessed by the pump pulse at different wavelengths are distinct enough to produce vastly different outcomes, as reflected by the pump dependence of the ESA features of the 1 ( T 1 T 1) and CT states.

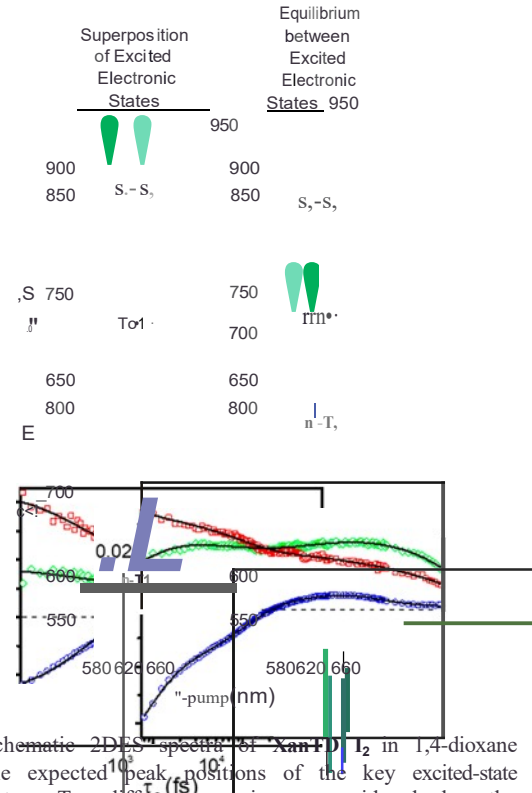


Figure 4. Schematie 2D 5 specific of Xant p 12 in 1,4-dioxane exhibiting the expected peak positions of the key excited-state absorption features. Two different scenarios are considered where the excited electronic states are a superposition of pure states (left) and when they are in equilibrium (right). The pump wavelength dependence of the ESA features is highlighted by two different elliptical shapes, mimicking the centers of the peaks observed in the linear absorption spectrum. While all the ESA features should peak close to the 0-0 vibronic peak center when the pure electronic states are in equilibrium (right), they can be centered at different pump wavelengths if the initially excited state is a superposition of the pure states (left), as observed experimentally.

Kinetic analyses were performed to further analyze the nature of the excited electronic states and explain the pump wavelength dependent dynamics of the 2DES spectral features observed for  $\mathbf{XanTD1_2}$  in 1,4-dioxane. The evolving states at all pump wavelength comprise mixed  $^1(S S_0)$ .  $^1(T_1 T_1)$  and CT contributions. Consequently, the excited-state dynamics of  $\mathbf{XanTD1_2}$  in 1,4-dioxane will be discussed in terms of which electronic states,  $^1(S S_1)$ .  $^1(T_1 T_1)$  or CT, dominate. Two

1 1

pump wavelength slices were chosen from the 2DES spectra at 609 and 650 nm, corresponding approximately to the centers of the ESA features arising from TDI and the 1(T T) states, respectively. Evolution-associated spectra (EAS) calculated from these pump wavelength slices of waiting time-dependent 2DES spectra are shown in Figure SA, while Table 1 lists the time constants related to the spectral changes along with the

processes leading to such changes. The corresponding decayassociated spectra (DAS) are given in Figure S6. Components in EAS analysisare distinguished by their kinetics. The 650 nm spectral slice can be fit to an A B c o model. The EAS reveal mixed  ${}^{1}(S_{1}S_{0}, {}^{1}(T_{1}T_{1})$  and CT character for all the states involved in the evolution, with different degrees of mixing. The initially excited state A is mostly  ${}^{1}(S_{1}S_{0})$ , with so me CT character as reflected by the ESAat 765 nm. State A converts to state B that contains more  ${}^{1}(T_{1}T_{1})$  character. Subsequently, the  ${}^{1}(T_{1}T_{1})$  contribution is further enriched, while that of  ${}^{1}(S_{1}S_{0})$  is diminished, with the CT contribution largely unchanged in state C. Given that maximal growth of the  $T_0$   $T_1$  ESA absorption is observed in state C, the conversion ofstate A into state C is the primary SF event that proceedsvia an intermediatestate B. Spectral changesbetween states C and D are minimal and this conversion primarily corresponds to the orientational relaxation of the XanTD12 molecule.

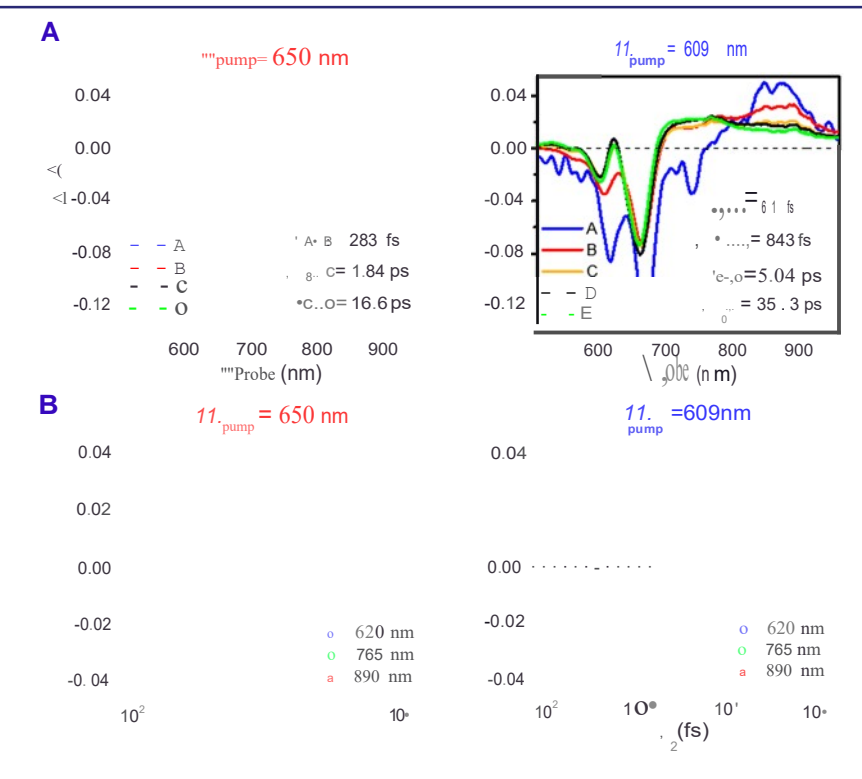


Figure S. Evolution-associated spectra and kinetics of XanTDI $_2$  in 1,4-dioxane. (A) Evolution-associated spectra of XanTDI $_2$  in 1,4-dioxane derived from 6SO and 609 nmpump wavelength slices of the 2DES spectra. (B) Kinetic fit to the data at 620 nm (T  $_{0}$ --T  $_{1}$  ESA transition), 76S nm (TDI.. ESA) and 890 nm (S  $_{0}$ --S  $_{1}$  ESA transition) probe wavelengths. The symbols (circle, diamond and square) represent the raw data and the black traces are the corresponding fits to the kinetic model.



Ta ble 1. T im e Constant's and Prim ary Photophysical Process Corresponding to the Evolution of States for XanTDI<sub>2</sub> in 1,4-Dioxane and DCM Based on Kinetic Fits to the Data

	ox	

run Pump Process	Time constant	50 nm Pump		
Process	Time constant			
	Time constant	Process		
Solvent relaxation	$283 \pm 22 \text{ fs}$	SF Intermediate formation		
Primary SF event	$1.84 \pm 0.13 \text{ ps}$	Primary SF event		
Orientational Relaxation	$16.6 \pm 3.1 \text{ ps}$	Orientational Relaxation		
Structural relaxation				
Dichloro	omethane			
609 nm Pump		650 run Pump		
Process	Time constant	Process		
SF Intermediate formation	$183 \pm 11 \text{ fs}$	SF intermediate formation		
Primary SF event	$935 \pm 61 \text{ fs}$	Primary SF event		
SB-CS	$10.5 \pm 2.3 \text{ ps}$	SB-CS		
	Primary SF event Orientational Relaxation Structural relaxation Dichloro  nm Pump  Process SF Intermediate formation Primary SF event	Primary SF event $1.84 \pm 0.13$ psOrientational Relaxation $16.6 \pm 3.1$ psStructural relaxationDichloromethanenm PumpProcessTime constantSF Intermediate formation $183 \pm 11$ fsPrimary SF event $935 \pm 61$ fs		

Assignment of this dynamical change is obtained from the decay of the polarization anisotropy of the 2DES signal at (JpumP',\robe)= (650 nm, 620 nm) (Figure S9C; 2DES spectra at perpendicular polarization and the EAS from them is shown in Figure S9A,B). State D persists for times longer than our measurement window.

In contrast, the 609 nm spectral slice requires an additional process(E) to fit properly. Here, the initially excited state, A, is an almost pure  ${}^{1}(S_{1}S_{0})$  state convoluted with the solvent response. Owing to the stronger pump intensity at 609 nm compared to 650 nm, the solvent respo nse is more intense in the initially excited state A at 609 nm pump wavelength. Thus, the solvent relaxation predominantly contributes to conversion of state A to state B, which shows strong CT character in conjunction with some (TT) and less (SS). The reafter, the system evolves to a (TT) where the (TT) character state C, (TT)grows significantly and both <sup>1</sup>(S<sub>1</sub>S<sub>0</sub>) and CT contributions are further reduced. Similar to the 650 nm spectral slice, evolution of the system into state C is the primary event of SF. State C subsequently converts into state D along with orientational relaxation of XanTDI21 as observed from the decay of the polarization anisotropy (Figure S9C). Finally, state D converts to state E where a slight decrease of the 1 (T<sub>1</sub>T<sub>1</sub> and 1 (S<sub>1</sub>S<sub>0</sub> con tr ibutio n s is observed, likely due to a structural relaxatio n within XanTDI2.637 Spectra of the states C, D and E are not significantly different since neither the orientational relaxatio n (in the lab frame) nor the structural relaxation (in the molecular frame) process results in changes in the electronic characteristics of the state. However, minor changes in the character of the mixed state on the time scale of orientational or structural relaxation cannot be ruled out based on subtle changes in the spectra of states C, D and E. The time scales we observe for these changes, in addition to c D conversion in the 650 nm slice, convolute the evolution of the state vector along with the orientational or structural relaxation process. Given that the time-resolved fluorescence spectrum of **XanTDI<sub>2</sub>** in 1,4-dioxane exhibits a lifetime of 1.58 ns,3 some <sup>1</sup>(S<sub>1</sub>S<sub>0</sub>) contribution is expected even at the final state of the evolution process, irrespective of the excitation wavelength.

In general, evolving states of this system can be represented as vectors in three-dimensional state space with  ${}^{1}(S_1S_0)$ , <sup>1</sup> (T<sub>1</sub>T<sub>1</sub>) and CT b asis states, as shown in Figure 6, where the projection of the vector along each axis gives the coefficient of the pure electronic state wavefunction. Population transfer alters the direction of the state vector but never projects onto

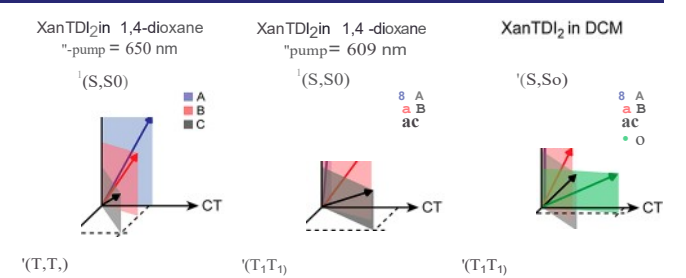


Figure 6 Vector representation of the electronic states with mixed <sup>1</sup>(S<sub>1</sub>S<sub>0</sub>), <sup>1</sup>(T<sub>1</sub>T<sub>1</sub>) and **er** characters during different stages of SF and SB-CS in XanTD lz. For XanTDI2 in 1,4-dioxane, evolution of the mixed electronic state vector is strongly dependent on the excitation wavelength, as observed from the left and center diagrams. Such excitation wavelength dependence is absent for XanTDI2 in DCM (right) during SB-CS. The dashed lines are used to indicate the  $(T, T_1)$  and  $\mathbf{C}\mathbf{r}$  character of the final states shown in each of the diagrams.

the basis planes, while population relaxation merely shortens the length of the vector. Though quantificatio n of the individual state contributions in the mixed states would be useful, the nature of the spectral features makes such an analysis challenging, as discussed in the Supporting Information (Section 9). Comparison of the EAS at different pump wavelengths shows some important differences. The final state of the system has more  ${}^{1}(T_{1}T_{1})$  and less CT character when pumped at 650 nm as opposed to 609 nm pump. The trend of decreasing <sup>1</sup>(T<sub>1</sub>T<sub>1</sub>) character with a corresponding increase in CT character in the terminal electronic state at shorter pump wavelengths is further established by carrying out EAS analysis on 2DES spectra collected using pump pulses that partially covers the 0-1 and 0-2 vibronic transitions (centered at 572 nm, see Figure Sll ). This indicates that the initially excited electronic state is part of a manifold of electronic states with varying mixed characters.

The primary event of SF is effectively evolution of the system into state C, which occurs in -r = 1.84 ps <sup>37</sup> via a twostep processwhen pumped at 650 nm as opposed to -r = 843 fs us in g a 609 nm pump. Thus, SF in XanTDI<sub>2</sub> in 1,4-dioxane converts a  ${}^{1}(S_1S_0)$ -dominant state into a  ${}^{1}(T_1T_1)$ -dominant one, which also has significant CT character. In addition, the <sup>1</sup>(T<sub>4</sub>T<sub>4</sub>) and CT contributions to the SF product state and the intermediate states are strongly dependent on excitation energy. A previous study of SF in TIPS-tetracene nanoparticles

found evidence for excitation dependent multiexciton stateJs however, the exact nature of those states remained unclear.<sup>3</sup> Furthermore, all the 2DES spectral features slightly red-shift as a function of waiting time, indicating the same intermediate states cannot be reached starting from different initial states. The pure  ${}^{1}(S_{1}S_{0})$ ,  ${}^{1}(T_{1}T_{1})$  and CT states are very close in energy, however, the electronic coupling in the system is weak.6 Thus, the low-frequency vibrational modes of the molecule may be responsible for mixing the electronic states, resulting in a manifold of vibronic states with varying electronic characters. With increase in energy, the partial <sup>1</sup>(T<sub>1</sub>T<sub>1</sub>) character decreases and the CT character increases in the manifold resulting in the observed evolution of the states as a function of excitation energy. Such a manifold of excited vibronic states may also convolute the vibrational relaxation process with the time scales for evolution of the mixed states when the 0-1 vibronic band is excited. Additionally, weak oscillations (-2-3 ps period) are observed in the kinetic traces of XanTDI 2 in 1,4-dio xane that survive for a few tens of ps (Figure SB). Given the very lowfrequency of these oscillations and their occurrence in both 1,4-dioxane and DCM (Figure S7), they may arise from interchromophore vibrations or librations of XanTDI2 and can potentially contribute to mixing of the pure electronic states. Detailed theoretical modeling is necessary to determine the nature of the vibrational mode(s) involved in the process that leads to such a vibronic manifold, and is beyond the scope of this work.

In DCM on the other hand, besides the features pertaining to the  ${}^{1}(S_{1}S_{0})$  state and TD1+•, the 2DES spectrum of **XanTDI<sub>2</sub>** at i-2 = 6 ps shows an ESA feature arising from the  $^{1}(T_{1}T_{1})$  state detected at 620 nm (Figure 3). This feature is overshadowed by the stronger GSB features. This is indicative of the  ${}^{1}(T_{1}T_{1})$  state or a mixed state with dominant  ${}^{1}(T_{1}T_{1})$ character being an intermediate during SB-CS. Also, there is no distinguishable pump wavelength dependence to the spectral features of XanTDI 2 in DCM as opposed to in 1,4-dioxane.

We have calculated the EAS (Figure S7) and DAS (Figure S8) taking slices at 609 and 650 nm pump wavelengths from the 2DES spectra in DCM. As indicated by the raw data, differences between the EAS calculated from the 650 nm and the 609 nm slices are subtle. Dynamics at each pump wavelength are well described by the same kinetic model. As summarized in Figure 6, the system starts from a state A that is largely  ${}^{1}(S_{1}S_{0})$  and evolves into state D with primarily CT character via two intermediate states, B and C. Both <sup>1</sup>(T<sub>1</sub>T<sub>1</sub>) and CT character increase monotonically in B and C. Finally, state C is converted to state D where the  ${}^{1}(T_{1}T_{1})$  character is reduced and CT character is gained. Most importantly, we observe an intermediate state C with significant (T )

character during the SB-CS for XanTDI 2 in DCM (Figures S7 and S8). Evolution of the system from state A into C via Bis the primary event of SF of XanTDI 21 similar to 1,4-dioxane, and generation of such a multiexciton state is independent of solvent polarity. Additionally, evolution of the system into state D is the effective SB-CS process, which occurs over "10 ps time period.<sup>37</sup>

Vibronic coupling within XanTDI2 in DCM does not appear to alter the nature of the excited electronic states of the system significantly as opposed to in 1,4-dioxane,as reflected through the lack of excitation wavelength dependence of the 2DES spectral features. We attribute this to the higher polarity of DCM lowering the CT state energy substantially compared to the  ${}^{1}(S_{1}S_{0})$  and  ${}^{1}(T_{1}T_{0})$  stat es. In other words, the initially

excited eigenstate vector remains largely unperturbed in the pure state basis (Figure 6), regardless of the number of vibrational quanta. However, evidence of mixed <sup>1</sup>(S<sub>1</sub>S<sub>0</sub>), CT and 1(T<sub>1</sub>T<sub>1</sub>) contributions in the intermediate states also implies that vibronic coupling is not inconsequential in this system because the relatively weak electronic coupling of the system is insufficient to cause such mixing. Theoretical studies may be able to identify relevant vibrational states and investigate the role of the optically allowed vibronic modes.

#### **CONCLUSIONS**

2DES studies on XanTDI2 show that despite weak electronic coupling, strong vibronic coupling yields mixed excited electronic states in this system. In nonpolar 1,4-dioxane, the  $^{1}(S_{1}S_{0})$  state evolves into mixed states having  $^{1}(S_{1}S_{0})$ ,  $^{1}(T_{1}T_{1})$ and CT character. Moreover, the <sup>1</sup>(T<sub>1</sub>T<sub>1</sub>) and the CT character of the evolving states depends strongly on excitation wavelength as a result of vibronic coupling. Thus, the usual notion of SF as transformation of <sup>1</sup>(S S)<sub>1</sub>to<sub>1</sub> <sup>1</sup>(T T) demands modification in such systems, necessitating a description in terms of electronic states with varying contributions from basis states. In polar DCM, XanTDI2 undergoes SB-CS via an intermediate state that is predominately <sup>1</sup>(T<sub>1</sub>T<sub>1</sub>). Therefore, we conclude that multiexciton state formation takes place in XanTDI2 regardless of the solvent polarity; however, a lower energy CT state in polar solvents is the final excited state formed. The change of the CT state energy influences the effect of vibronic coupling of the system as well, resulting in no significant excitation wavelength dependence of the dynamics in polar DCM These results provide important insights into the nature of the multiexciton state, as well as input for theoretical modeling studies of SF that take into account the complex interplay between electronic energies and couplings present in these systems.

# **METHODS**

The synthesis of XanTDI and XanTDI was described earlier.3<sup>7</sup> 1,4 -Dioxane was purified by distillation over LiAll4 to remove peroxides, while DCM was purified and dried with a Pure Process Technology solvent purification system. Dilute solutions (- 10- 6M) of XanTDI<sub>2</sub> in 1,4-dioxane or DCM were typically employed in the 2DES experiments.

The femtosecond pump pulses were generated using a P-barium borate (BBO) based two-stage noncollinear optical parametric amplifier (Spirit-NOPA, Light Conversion Inc.). The NOPA was pumped by the fundamental output of a Yb:KGW regenerative amplifier (Spirit, Spectra Physics, 1040-4) with a 104-0 nm, 400 fs, 22  $\mu J$  pulse at a 100 kHz repetition rate. A small portion of the 1040 nm input into the NOPA (-HJ%) is used to create a white light seed using a YAG crystal. The remaining 1040 nm input is converted to its third harmonic (347 nm) using BBO crystals and used to amplify the white light seed noncollinearly using a two-stage BBO-based amplifier. For the experiments described in this work, the pump pulse is centered at -620 nm with a bandwidth (fuJJ width at half-maximum) of -1080 cm-•. A portion of the 104-0 nm output of the regenerative amplifier (-2.S  $\mu$ ]/pulse) is focused into a 4 mm thick YAG crystal using a 100 mm f.l. lens to generate a white light pulse that spans -490-1000 nm. The white light is collimated using an off-axis parabolic mirror (100 mm £1.) and a 104-0 nm notch filter is used to remove the residual fundamental 104-0 nm light. Thereafter, secondorder dispersion in the white light is compensated for using a pair of chirped mirrors (Layertec Inc., 16 bounces, +40 fs<sup>2</sup> mm between 500 and 1000 nm). This white light pulse is used as the probe in the 2DES measurements. Frequencyresolvedoptical gating (FROG) measure-

**MMM** 

ments were used to determine the -45 fs overall instrument response function (Figures SI and S2, Supporting Information).

The 2DES experiments were performed using a commercial 20 spectrometer (2DQuickVIS, Phasetech Spectroscopy, Inc.), which utilizes the pump-probe geometrywith a pulse shaper to generate the time-orderedpumppulses. Useof a pulseshaper ensures that the time overlap of the two pump pulses is known accurately so that no phasing of the data is needed during postprocessing. The pulse shaper also compensates for dispersion of the pump pulses, particularly thirdorder dispersion. Four-frame phase cycling is employed to collect the 2DES i ectra, which efficiently removes pump scatter from the spectra. In this configuration, two collinearly propagating timeordered pump pulses first interact with the sample, followed by the white light probe pulse. The third-order nonlinear signal is emitted in the phase-matched direction of the probe pulse. The signal is detected by self-heterodyning with the probe, spectrally dispersed using a monochromator, and imaged on a CCD line camera. The delay between the two pump pulses and the probe pulse is scanned and the probe spectrum is recorded at each delay. This produces the probe wavelength data, while the pump wavelength data is obtained by numerical Fourier transformation of the coherence time, -r during postprocessing of the data.

## ASSOCIATED CONTENT

# **0** Support ing Information

The Supporting Information is available free of charge on the ACS Publications website at DOI: 10.1021/ jacs.8b08627.

Experimental details and characterization (PDF)

#### AUTHOR INFORMATION

## **Corresponding Authors**

\*m-wasielewski@)north western.edu

\*ryan.young@)north western.edu

## ORCID CD

Ari tra Man dal: 0 000--0002-8680-3730 Ryan M. Young: 0000-0002-5108-0261 Martin T. Zanni: 0000-00017191-9768

Mi chae 1 R W asielew ski: 0000-0003-2920-5440

## Notes

The authors declare the following competing financial interest(s): M.T.Z. is an owner of PhaseTech Spectroscopy, Inc.

# ACKNOWLEDGMENTS

This work was supported by the U.S. Department of Energy, Office of Science, Office of Basic Energy Sciences under Award DE-FG02-99ER14999 (M.R.W., synthesis, data acquisition and analysis) and by the National Science Foundation under Grant CHE-1665110 (M.T.Z., instrument design and data analysis). M.C. gratefully acknowledges support from the Ryan Fellowship and the Northwestern University International Institute for Nanotechnology.

## REFERENCES

- (1) Hanna, M. C.; Nozik, A J. Solar Conversion Efficiency of Photovoltaic and Photoelectrolysis Cells with Carrier Multiplication Absorbers. J. Appl. Phys. 2006, 100, 074510.
- (2) Smith, M. B.; Michl, J. Singlet Fission. *Chem. Rev.* 20 10, *110*, 6891-6936.
- (3) Smith, M. B.; Michl, J. Recent Advances in Singlet Fission. *Annu. Rev. Phys. Chem.* 2013, 64, 361-386.
- (4) Rao, A; Friend, R H. Harnessing Singlet Exciton Fission to Break the Shockley-Q ueisser Limit. *Nat. Rev. Mater.* 2017, 2, 17063.

- (5) Eaton, S. W.; Shoer, L. E.; Karlen, S. D.; Dyar, S. M.; Margulies, E. A; Veldkamp, B. S.; Ramanan, C.; Hartzler, D. A; Savikhin, S.; Marks, T. J.; Wasielewski, M. R Singlet Exciton Fission in Polycrystalline Thin Films of a Slip-Stacked Perylenediirnide. J. Am. Chem. Soc. 201 3, 135, 14701-14712.
- (6) Margulies, E. A.; Miller, C. E.; Wu, Y.; Ma, L.; Schatz, G. C.; Young, R M.; Wasielewski, M. R Enabling Singlet Fission by Controlling Intramolecular Charge Transfer in Jr-Stacked Covalent Terrylenediirnide Dimers. *Nat. Chem.* 2016, 8, 1120-1225.
- (7) Fuemmeler, E. G.; Sanders, S. N.; Pun, A B.; Kumarasamy, E.; Zeng, T.; Miyata, K; Steigerwald, M. L.; Zhu, X Y.; Sfeir, M. Y.; Campos, L. M.; Ananth, N. A Direct Mechanism of Ultrafast Intramolecular Singlet Fission in Pentacene Dimers. ACS Cent. Sci. 2016, 2, 316-324.
- (8) Margulies, E.A.; Logsdon, J. L.; Miller, C. E.; Ma, L.; Simonoff, E.; Young, R. M.; Schatz, G. C.; Wasielewski, M. R. Direct Observation of a Charge-Transfer State Preceding High-YieldSinglet Fission in Terrylenediirnide Thin Films. J. Am. Chem. Soc. 2017, 139, 663-671.
- (9) Le, **A.** K; Bender, J. A; Arias, D. H.; Cotton, D. E.; Johnson, J. C.; Roberts, S. T. Singlet Fission Involves an Interplay between Energetic Driving Force and Electronic Coupling in Perylenediirnide Films. J. Am. Chem. Soc. 2018, 140, 814-826.
- (10) Greyson, E. C.; Stepp, B. R; Chen, X.; Schwerin, A. F.; Paci, I.; Smith, M. B.; Akdag, A; Johnson, J. C.; Nozik, A. J.; Michl, J.; Ratner, M. A. Singlet Exciton Fission for Solar Cell Applications: Energy Aspects of Interchromophore Coupling. J. Phys. Chem. B 2010, 114, 14223-14232.
- (11) Zimmerman, P. M.; Zhang, Z.; Musgrave, C. B. Singlet Fission in Pentacene through Multi-Exciton Quantum States. *Nat. Chem.* 2010, 2, 648-652.
- (12) Zimmerman, P. M.; Bell, F.; Casanova, D.; Head-Gordon, M. Mechanism for Singlet Fission in Pentacene and Tetracene: From Single Exciton to Two Triplets. J. Am. Chem. Soc. 2011, 133, 19944-19952.
- (13) Chan, W.-L.; Berkelbach, T. C.; Provorse, M. R; Monahan, N. R; Tritsch, J. R; Hybertsen, M.S.; Reichman, D. R; Gao, J.; Zhu, X Y. The Quantum Coherent Mechanism for Singlet Fission: Experiment and Theory. Acc. Chem. Res. 201 3, 46, 1321-1329.
- (14) Monahan, N.; Zhu, X. Y. Charge Transfer-Mediated Singlet Fission. Annu. Rev. Phys. Chem. 2015, 66, 601-618.
- (15) Berkelbach, T. C.; Hybertsen, M. S.; Reichman, D. R. Microscopic Theory of Singlet Exciton Fission. I. General Formulation. J. Chem. Phys. 20 13, 138, 114102.
- (16) Berkelbach, T.  $\dot{C}$ .; Hybertsen, M. S.; Reichman, D. R. Microscopic Theory of Singlet Exciton Fission. II. Application to Pentacene Dimers and the Role of Superexchange. J. Chem. Phys. 2013, I38, I14103.
- (17) Morrison, A. F.; Herbert, J. M. Evidence for Singlet Fission Driven by Vibronic Coherence in Crystalline Tetracene. *J. Phys. Chem. Lett.* 2017, *8*, 1442-1448.
- (18) Bakulin, A A; Morgan, S. E.; Kehoe, T. B.; Wilson, M. W. B.; Chin, A. W.; Zigmantas, D.; Egorova, D.; Rao, A. Real-Time Observation of Multiexcitonic States in Ultrafast Singlet Fission Using Coherent 20 Electronic Spectroscopy. *Nat Chem.* 2016, 8, 16-23.
- (19) Musser, A J.; Liebel, M.; Schnedermann, C.; Wende, T.; Kehoe, T. B.; Rao, A.; Kukura, P. Evidence for Conical Intersection Dynamics Mediating Ultrafast Singlet Exciton Fission. Nat Phys. 2015, 11, 352-357.
- (20) Tempelaar, R; Reichman, D. R Vibronic Exciton Theory of Singlet Fission. I. Linear Absorption and the Anatomy of the Correlated Triplet Pair State. *J. Chem. Phys.* 201 7, *146*, 174703.
- (21) Tempelaar, R; Reichman, D. R Vibronic Exciton Theory of Singlet Fission. II. Two-Dimensional Spectroscopic Detection of the Correlated Triplet Pair State. *J. Chem. Phys.* 2017, *146*, 174704.
- (22) Burdett, *J.J.*; Bardeen, C. J. The Dynamics of Singlet Fission in Crystalline Tetracene and Covalent Analogs. *Acc. Chem. Res.* 201 3, 46, 1312-1320.

- (23) Basel, B. S.; Zirzlmeier, J.; Hetzer, C.; Reddy, S. R; Phelan, B. T.; Krzyaniak, M. D.; Volland, M. K; Coto, P. B.; Young, R. M.; Oark, T.; Wasielewski, M.; Thoss, M.; Tykwinski, R R; Guidi, D. M. Evidence for Charge-Transfer Mediation in the Primary Events of Singlet Fission in a Weakly Coupled Pentacene Dimer. Chem. 2018, 4, 1()()2-1111.
- (24) Margulies, E. A; Wu, Y.-L.; Gawel, P.; Miller, S. A.; Shoer, L. E.; Schaller, R D.; Diederich, F.; Wasielewski, M. R Sub-Picosecond Singlet Exciton Fission in Cyano-Substituted Diaryltetracenes. Angew. Chem, Int. Ed. 201S, 54, 8679-8683.
- (25) Grieco, C.; Kennehan, E. R; Kim, H.; Pensack, R D.; Brigeman, A N.; Rirnshaw, A; Payne, M. M.; Anthony, J. E.; Giebink, N. C.; Scholes, G. D.; Asbury, J. B. Direct Observation of Correlated Triplet Pair Dynamics During Singlet Fission Using Ultrafast Mid-IR Spectroscopy. J. Phys. Chem. C 2018, 122, 2012-2022.
- (26) Pensack, R D.; Ostroumov, E. E.; Tilley, A. J.; Mazza, S.; Grieco, C.; Tho rley, K J.; Asbury, J. B.; Seferos, D. S.; Anthony, J. E.; Scholes, G. D. Observation of Two Triplet-Pair Intermediates in Singlet Exciton Fission. J. Phys. Chem. Lett. 2016, 7, 2370-2375.
- (27) Breen, I.; Tempelaar, R; Bizimana, L. A; Kloss, B.; Reichman, D. R; Turner, D. B. Triplet Separation Drives Singlet Fission after Femtosecond Correlated Triplet Pair Production in Rubrene. J Am. Chem. Soc. 201 7, 139, 11745-11751.
- (28) Hart, S. M.; Silva, W. R; Frontiera, R R Femtosecond Stimulated Raman Evidence for Charge-Transfer Character in Pentacene Singlet Fission, Chem. ScL 2018, 9, 1242-1250.
- (29) Lee, J.; Bruzek, M. J.; Thompson, N. J.; Sfeir, M. Y.; Anthony, J. E.; Baldo, M. A Singlet Exciton Fission in a Hexacene Derivative. Adv. Mater. 2013, 25, 1445-1448.
- (30) Sanders, S. N.; Kumarasamy, E.; Pun, A. B.; Trinh, M. T.; Choi, B.; Xia, J.; Taffet, E.J.; Low, J. Z.; Miller, J. R.; Roy, X.; Zhu, X.Y.; Steigerwald, M. L.; Sfeir, M. Y.; Campos, L. M. Quantitative Intramolecular Singlet Fission in Bipentacenes. J. Am. Chem. Soc. 20 15, 137, 8965-8972.
- (31) Le, A. K; Bender, J. A.; Roberts, S. T. Slow Singlet Fission Observed in a Polycrystalline Perylenediirnide Thin Film. J Phys. Chem. Lett. 2016, 7, 4922-4928.
- (32) Mauck, C. M.; Bae, Y. J.; Chen, M.; Powers-Riggs, N.; Wu, Y. L.; Wasielewski, M. R Charge-Transfer Character in a Covalent Diketopyrrolopyrrole Dimer: Implications for Singlet Fission. ChemPhotoChem, 2018, 2, 223-233.
- (33) Miller, C. E.; Wasielewski, M. R; Schatz, G. C. Modeling Singlet Fission in Rylene and Diketopyrrolopyrrole Derivatives: The Role of the Charge Transfer State in Superexchange and Excimer Formation. J. Phys. Chem. C 2017, 121, 10345- 10350.
- (34) Johnson, J.C.; Akdag, A; Zamadar, M.; Chen, X.; Schwerin, A F.; Paci, I.; Smith, M. B.; Havlas, Z.; Miller, J. R; Ratner, M. A.; Nozik, A. J.: Michl, J. Toward Designed Singlet Fission: Solution Photophysics of Two Indirectly Coupled Covalent Dimers of 1,3-Diphenylisobenzofuran. *J. Phys. Chem. B* 2013, *117*, 4680-4695.
- (35) Ryerson, J. L.; Schrauben, J. N.; Ferguson, A. J.; Sahoo, S. C.; Naumov, P.; Havlas, Z.; Michl, J.; Nozik, AJ.; Johnson, J. C. Two Thin Film Polymorphs of the Singlet Fission Compound 1,3-Diphenylisobenzofuran. *J. Phys. Chem.* C 2014, *118*, 12121-12132.
- (36) Schrauben, J. N.; Ryerson, J. L.; Michl, J.; Johnson, J. C. Mechanism of Singlet Fission in Thin Films of 1,3-Diphenylisobenzofuran. J. Am. Chem. Soc. 2014, 136, 7363-7373.
- (37) Chen, M.; Bae, Y. J.; Mauck, C. M.; Mandal, A; Young, R. M.; Wasielewski, M. R Singlet Fission in Covalent Terrylenediimide Dimers: Probing the Nature of the Multiexciton State Using Femtosecond Mid-Infrared Spectroscopy. J Am. Chem. Soc. 20 18, 140, 9184-9192.
- (38) Middleton, C. T.; Woys, A. M.; Mukherjee, S. S.; Zanni, M. T. Residue-Specific Structural Kinetics of Proteins through the Union of Isotope Labeling, Mid-IR Pulse Shaping, and Coherent 20 IR Spectroscopy. Methods 2010, 52, 12- 22.
- (39) Thampi, A.; Stem, H. L.; Cheminal, A; Tayebjee, M. J. Y.; Petty, A J.; Anthony, J. E.; Rao, A Elucidation of Excitation Energy Dependent Correlated Triplet Pair Formation Pathways in an

- Endothermic Singlet Fission System. J. Am. Chem. Soc. 2018, 140, 4613-4622.
- (40) Yan, S.: Tan, H.-S. Phase Cycling Schemes for Two-Dimensional Optical Spectroscopy with a Pump-Probe Beam Geometry. Chem. Phys. 2009, 360, 110-115.